Title	Analysis of a Record-Breaking Strong Wind Event at Syowa Station in January 2015
Authors	Yamada Kyohei, Hirasawa Naoki
Citation	JGR: Atmospheres, 123(24), 13,643-13,657, 2018
Issue Date	2018-11-12
Type	Journal Article
URL	https://doi.org/10.1029/2018JD028877
Right	
Textversion	publisher

Journal of Geophysical Research: Atmospheres

RESEARCH ARTICLE
10.1029/2018JD028877

Analysis of a Record-Breaking Strong Wind Event at Syowa Station in January 2015

K. Yamada[1] and N. Hirasawa[1]

[1]National Institute of Polar Research, Tachikawa, Japan

Key Points:
- Syowa Station in Antarctica observed record-breaking strong surface wind on 17 January 2015
- In WRF simulations the strong surface wind is accelerated by a relationship with the geostrophic wind called *orographic blocking*
- Orographic blocking with an easterly low-level jet is caused by a strong northerly associated with a synoptic-scale depression

Correspondence to:
K. Yamada,
yamada.kyohei@nipr.ac.jp

Citation:
Yamada, K., & Hirasawa, N. (2018). Analysis of a record-breaking strong wind event at Syowa Station in January 2015. *Journal of Geophysical Research: Atmospheres*, *123*, 13,643–13,657. https://doi.org/10.1029/2018JD028877

Received 27 APR 2018
Accepted 4 NOV 2018
Accepted article online 12 NOV 2018
Published online 20 DEC 2018

Abstract Syowa Station in Antarctica observed a January record strong surface wind on 17 January 2015 with a maximum mean wind speed of 41.8 m/s. The strong wind event is studied here using the Weather Research and Forecasting model. The event occurred under the influence of enhanced northerly wind associated with an intense synoptic-scale depression that approached the west of Syowa station. The northerly wind turned easterly along the coast of the ice sheet with remarkable near-surface acceleration. The acceleration of the surface wind at Syowa Station was connected with the establishment of the easterly low-level jet that formed as a result of *orographic blocking* as follows: (1) Air with low potential temperature around the southern end of the northerly wind was forced to ascend by the slope of the ice sheet; (2) the upwelling transported air from the lower atmosphere, resulting in the establishment of a cold region along the slope; (3) the deformed temperature structure generated a strengthening horizontal pressure gradient; and (4) the negative pressure gradient $\partial p/\partial y$ was larger at lower altitudes, resulting in stronger easterly wind in the lower layer, consistent with thermal wind balance. During the strong wind event, katabatic wind was enhanced by the greater katabatic force associated with the stronger negative pressure gradient. Another interesting feature was a local warming at surface level in Lutzow-Holm Bay. The warming was driven by a foehn mechanism. The other branch of the downslope wind upwelled again above the bay, and this upwelling extended up to the tropopause.

1. Introduction

The Antarctic surface wind is an important component of the Antarctic heat budget, surface mass balance, and hydrologic cycle (Bintanja, 1998; Bromwich et al., 1995; van den Broeke et al., 2005). Over the Southern Ocean, the circumpolar westerlies prevail throughout the year, forming the storm track with synoptic-scale disturbances migrating toward the Antarctic continent. Over the continent, radiative cooling of the surface results in katabatic wind. This downslope flow reaches its greatest speed over the coastal regions, where the ice sheet is steepest (Kodama et al., 1989; Parish & Bromwich, 1987).

The other factor influencing the surface wind is the synoptic-scale pressure gradient caused by cyclones from the storm track (Trenberth, 1991) and blocking anticyclones (Hirasawa et al., 2000, 2013). Knuth and Cassano (2011) analyzed near-surface wind and other conditions in Terra Nova Bay, Antarctica, from 1993 to 2009 using automatic weather station and satellite data. This region is subjected to strong downward flows, primarily in a westerly to northwesterly direction along the slope, in all seasons. Most strong wind events are concurrent with downward flows. An investigation of 15 strong wind events with wind speeds greater than 20 m/s that lasted for more than 10 hr revealed that all the events were caused by a depression over the adjacent Ross Sea. Simmonds et al. (2003) analyzed the National Centers for Environmental Prediction (NCEP) Department of Energy Reanalysis-2 data set with the cyclone tracking algorithm of the sophisticated Melbourne University cyclone tracking scheme (Simmonds et al., 1994; Simmonds & Murray, 1999) for high southern latitudes for the period January 1979 to February 2000. The cyclone system density (mean number of cyclones in a 10^3 [degree lat]^2 area per analysis) was highest near or to the south of 60°S. The cyclone system density in winter is generally greater than that in summer. Uotila et al. (2011) investigated the relationship between cyclone character and surface properties in Antarctic regions using the Antarctic Mesoscale Prediction System (AMPS; Powers et al., 2012) and the University of Melbourne Cyclone detection and tracking algorithm (Simmonds & Keay, 2000) for 2001 to 2009. They found that 20% of the cyclone systems were mesoscale and 80% were large synoptic systems. The number of each type of cyclone system increased in winter and decreased in summer. Cyclone properties are strongly correlated with surface properties, such as latent heat, sensible heat, and temperature

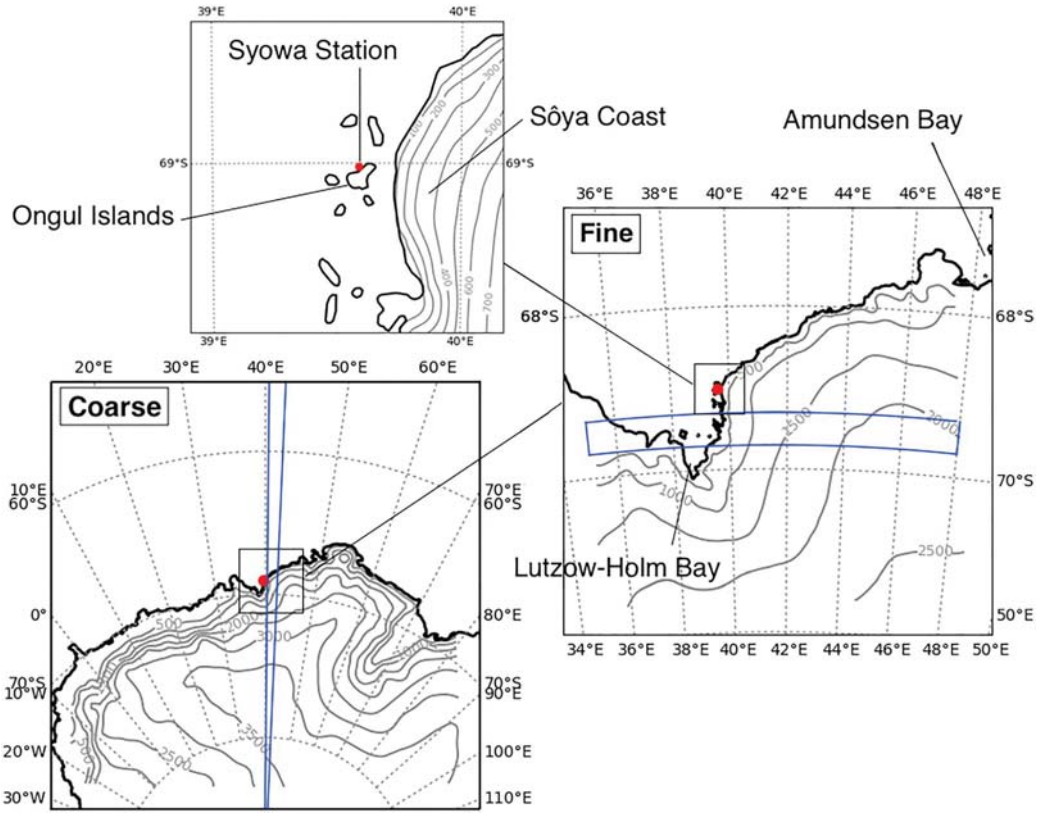

Figure 1. Domains of the Weather Research and Forecasting model calculations and geographic information for the region surrounding Syowa Station. Red circle indicates the location of Syowa Station. Blue outlines indicate the cross-section areas.

gradient. Hoskins and Hodges (2005) studied Southern Hemisphere storm tracks using 45 years of European Center for Medium Range Weather Forecasts (ECMWF) Reanalysis (ERA-40) data. They found that high-latitude storm tracks in summer took the shape of a single spiral. However, winter storm tracks were separated into a polar loop and a subtropical loop in both the lower and upper troposphere. The tracks in summer were located between the subtropical and polar winter loops. Summer track intensities were generally stronger than the polar loop but weaker than the subtropical loop of winter. In the transition season from summer to winter, storm track locations were similar to those during summer; however, the subtropical storm track builds gradually. In coastal regions, the surface wind is typically highly variable because of the combination of the katabatic effect, the synoptic-scale pressure gradient, and orographic conditions.

Syowa Station (69.0°S, 39.6°E; Figure 1), located on East Ongul Island in Lutzow-Holm Bay, Antarctica, is the main base of the Japanese Antarctic Research Expedition. Meteorological observations have been carried out at Syowa Station since 1957. On 17 January 2015, a strong wind event with a maximum mean wind speed (maximum value of 10-min average wind speed) of 41.8 m/s and gusts up to 51.4 m/s was observed at Syowa Station. This broke the January wind speed record at Syowa Station. Around the coast of East Antarctica, including Syowa station, most strong wind events are associated with enhancement of downslope katabatic flow by the synoptic circulation. Syowa Station has less frequent strong wind events than other coastal stations in the Eastern Antarctic region, such as Mirny (66.6°S, 93.0°E) or Davis (68.6°S, 78.0°E), because it is not located near the major confluence zones of the katabatic forcing and synoptic-scale pressure gradient forcing (Parish & Bromwich, 1987). The seasonal cycle of strong wind events shows a low frequency for summer season and high frequency from April to May associated with shifting of the storm track (Turner et al., 2009). According to Sato and Hirasawa (2007), the tropospheric westerly wind speed at Syowa Station has increased since the 1960s.

Strong wind events often occur at the same time as the approach of a strong depression, and a steep topography sometimes deflects the wind. Orr et al. (2014) studied a strong winter wind event at Mawson Station (67.6°S, 62.9°E), East Antarctica. A depression reached the station and the sea-level pressure fell by over 40 hPa at the time of the strong wind. The flow was deflected by the topography near the station and a barrier jet formed along the coastline. The combination of barrier jet and katabatic wind produced the strong wind. Chenoli et al. (2015) investigated a strong wind event at McMurdo Station (77.9°S, 166.7°E) and the Ross Island region on the Ross Ice Shelf using in situ observations, satellite imagery, numerical weather prediction, and reanalysis data. On 10 October 2003, when wind speed of 16 m/s was observed at McMurdo Station, there were three mesoscale low-pressure systems that passed from the central Ross Ice Shelf to the southwestern Ross Sea. In their early stages, with wind speed lower than 10 m/s, southerly winds caused primarily by one of the low-pressure systems were deflected by the topography of the Minna Bluff and Black and White Island. As the pressure gradient increased, southerly wind crossed the topography and mountain waves were formed along the lee slope. Finally, with a Froude number greater than 1, the vertical propagation of mountain waves was strengthened over McMurdo Station and wind speed reached a maximum. The amplification of the vertical propagation of mountain waves was caused by the large amount of energy associated with the enhanced downslope wind. O'Connor et al. (1994) investigated a strong wind event in the boundary layer near Ross Island (77.5°S, 167°E). The Transantarctic Mountains, with steep slopes and elevations above 2,000 m, are located to the west of Ross Island. When the strong wind event occurred, a cyclone approached the mountains and the cyclonic winds were deflected by the steep topography. The blocking caused a pressure gradient perpendicular to the mountains, which accelerated the wind along the topography as a result of the geostrophic effect (barrier winds). The barrier wind effect has frequently been discussed in the literature in regard to the Transantarctic Mountains and the Ross Ice Shelf. Nigro and Cassano (2014) also analyzed the surface wind patterns over the Ross Ice Shelf using with the Weather Research and Forecasting model (WRF) from AMPS. The authors used the method of self-organizing maps, which is a training method using a neural network algorithm, to identify the dominant 10-m wind patterns. Wind conditions over the Ross Ice Shelf varied and were classified into five patterns. The Ross Ice Shelf airstream was driven by a combination of katabatic winds, barrier winds, and synoptic cyclone forcing. In the region of the Ross Ice Shelf, the steep topography along the Transantarctic Mountains played the role of a barrier. At the end of a barrier or protrusion in the topography (northwest of the Prince Olav Mountains), barrier winds accelerated.

Strong wind events play a significant role in the heat budget of the troposphere and surface mass balance in Antarctic regions. Van As et al. (2007) analyzed strong wind events that occurred at Kohnen Station (75°00′S, 0°047′E) during the European Project for Ice Coring in Antarctica-Netherlands Atmospheric Boundary Layer Experiment. This region experiences frequent strong wind events caused by warm-core cyclones in the northeastern Weddell Sea. Because of the transportation of moisture and heat from the south Tasman Sea onto the Antarctic Plateau, the destruction of the surface-based temperature inversion, and significant cloud coverage that prevents radiative cooling, near-surface air temperature during strong wind events was higher than that throughout the year by 4–5 K in summer and ~16 K in winter. Increased temperatures affected half of the East Antarctic Plateau. Strong wind events also contributed to mass transport by snowdrift for friction velocity values larger than 0.25 m/s.>

Investigation and reproduction of strong wind events are important in the assessment of numerical forecast capabilities. Understanding strong wind events also contributes to public safety in Antarctic regions. Previous studies have investigated strong wind events caused by synoptic-scale depressions at several coastal stations; for example, at Casey Station (Adams, 2005; Turner et al., 2001) and McMurdo Station (Chenoli et al., 2013; Steinhoff et al., 2008). However, few studies have investigated strong wind events at Syowa Station. This study aims to document the strong wind event at Syowa Station in January 2015 and to investigate the mechanisms responsible using model simulations. The remainder of this manuscript is organized as follows. In section 2, we examine the surface meteorological conditions and characteristics of the surface wind at Syowa Station using in situ observations. A description of model calculations using the WRF is also given in this section. Section 3 presents the spatial structure of the wind, temperature, and pressure fields obtained from model calculations. On the basis of the analysis, the mechanism generating the strong wind is discussed. Section 4 presents a summary and conclusions.

2. Data and Analysis

2.1. Surface Wind Conditions at Syowa Station

Meteorological observations have been carried out at Syowa Station for more than 50 years, and the strong wind on 17 January 2015 broke the January record. Sato and Hirasawa (2007) analyzed the surface meteorological data for 50 years at Syowa Station and reported mean wind speed and directional constancy (i.e., the absolute value of the vector average divided by the scalar average for winds) of 6.6 m/s and 0.78, respectively. The first and second most frequently observed wind directions are northeasterly and southerly, respectively.

Figure 2 shows the observed hourly mean surface pressure, air temperature, horizontal wind speed, and wind direction at Syowa Station from 16 to 18 January 2015, and Figure 3 gives the mean surface air temperature, surface pressure, and wind at 0000 UTC from 16 to 18 January 2015 for the area immediately surrounding Syowa, derived from the ECMWF Interim Re-Analysis (ERA-Interim; Dee et al., 2011). Wind speed increased by around 8 m/s from 0000 to 1200 UTC on 16 January together with an increase in surface air temperature of about 4 K. These changes in temperature and wind speed are thought to have resulted from the approach of a depression that was accompanied by warm air migrating southward to the east and southeast of the depression. Then the pressure started to fall from around 0900 UTC on 16 January. From 1500 UTC to 2200 UTC on 16 January, wind speed increased rapidly, while the temperature rose a further 2 K while fluctuating. Wind speed reached its maximum of 40.3 m/s at 2200 UTC on 16 January and maintained high speeds of nearly 40 m/s for 4 hr. Pressure reached its minimum of 968.3 hPa at 0000 UTC on 17 January. Warm air advection is apparent in Figure 3b, when the depression is closest to Syowa Station. As the depression weakened and departed, the pressure then increased and wind speed decreased with time while the surface air temperature changed little. Figure 3c shows the conditions after the strong wind event. There is no area of low pressure around Syowa Station.

During 1959–2015, except for the period from 8 February 1962 to 3 January 1966 for which observations are unavailable, 50% of the recorded daily maximum wind speeds in January were below 9 m/s and 95% were below 21 m/s. Thus, a maximum wind speed over 40 m/s is a unique event. The lowest frequency of strong wind events (maximum wind speed of 7 and above on the Beaufort scale, which is 28 knots or 13.9 m/s, for at least 6 hr) was in January. Moderate wind in summer is a common feature of other stations on the East Antarctic coast; for example, Molodyozhnaya Station (67.7°S, 45.8°E) to the east of Syowa Station. The seasonal changes are influenced by the position of the storm track (Turner et al., 2009) and by variations in the katabatic wind. In general, the katabatic component becomes strong in winter months because of strong radiative cooling of the ice sheet surface, while enhanced solar heating in summer months weakens the katabatic component and decreases the frequency of influence of katabatic wind (Parish & Cassano, 2003).

2.2. Numerical Model

To analyze the wind field and meteorological conditions for the strong wind event, we reproduce the event in a simulation with the WRF model version 3.5 (Skamarock, 2008). Powers (2007) used the WRF to reproduce a strong wind event at McMurdo station on 15 May 2004 and demonstrated its good performance in polar analysis by comparison with the fifth-generation Pennsylvania State University-National Center for Atmospheric Research Mesoscale Model. In the present paper, the input data are the global analysis and forecast data of the NCEP Final Analysis (GFS-FNL; NCEP/National Weather Service/NOAA/U.S. Department of Commerce, 2000), with spatial and temporal resolution of 1° and 6 hr, respectively, and 26 vertical levels from 1,000 to 10 hPa. NCEP GFS-FNL incorporates observational data from the Global Data Assimilation System and other sources. The simulation is run from 15 to 19 January 2015 with 61 eta levels in the vertical. The time step is 180 s and nested domains are used. Domain-01 with 30-km resolution is the outermost area and contains Domain-02 with a spatial resolution of 10 km. Similarly, Domain-02 contains Domain-03 with a spatial resolution of 3.3 km. In the present paper, Domain-01 is generally used as the coarse domain, and Domain-03 is the fine domain (Figure 1). Table 1 lists the WRF calculation parameters. In the radiative transfer calculation, the Rapid Radiative Transfer Model—Global scheme for longwave radiation and the Goddard shortwave radiation scheme for shortwave radiation are used every 15 min. The model employs planetary boundary layer physics schemes that include the Mellor-Yamada-Janjic Scheme (Janjić, 1990) updated every time step, and the WRF Single Moment 5 Class (WSM5) cloud microphysics scheme (Hong et al., 2004). The surface layer scheme is the Monin-Obkhov scheme. The cumulus parameterization is the Kain-Fritsch parameterization in

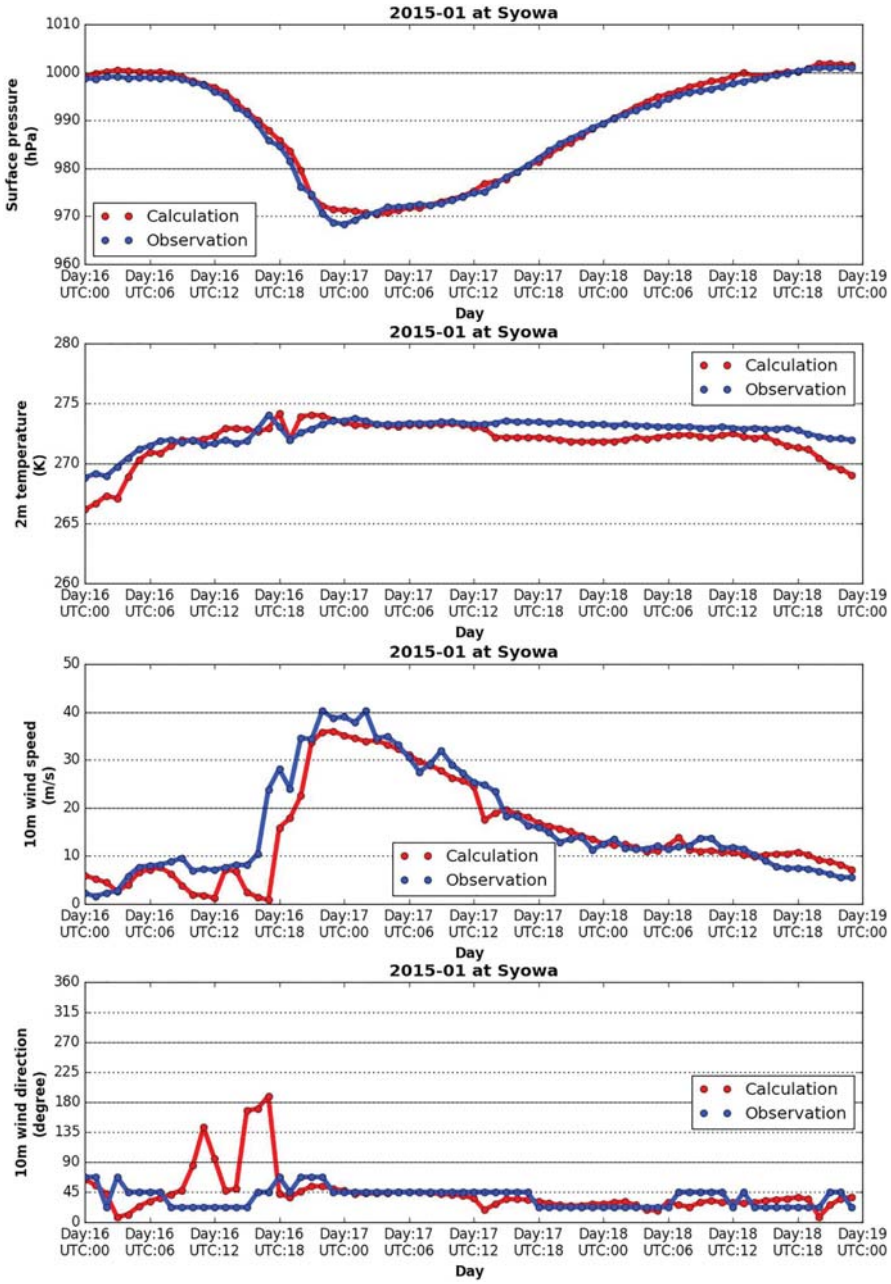

Figure 2. Surface pressure, surface air temperature, horizontal wind speed, and wind direction at Syowa Station from the Weather Research and Forecasting model simulation using the fine domain (red) and in situ observations (blue) from 16 to 18 January 2015.

the coarse domain, updated every time step. For the fine domain, no cumulus parameterization is used. Vertical velocity damping and nudging are not applied. Parameterizations of the physics, such as radiative processes, boundary layer processes, and cloud physics, are the same as those of AMPS. Sea surface temperatures and sea ice are adopted from GFS-FNL.

To calculate air back trajectories, the Meteorological Data Explorer (http://db.cger.nies.go.jp/metex/index.jp.html) developed at the Centre for Global Environmental Research using the method of Petterssen (1940) is applied. The horizontal and vertical coordinates used are longitude-latitude and pressure, respectively. Vertical interpolation is linear with geopotential height. The time step is determined according to the

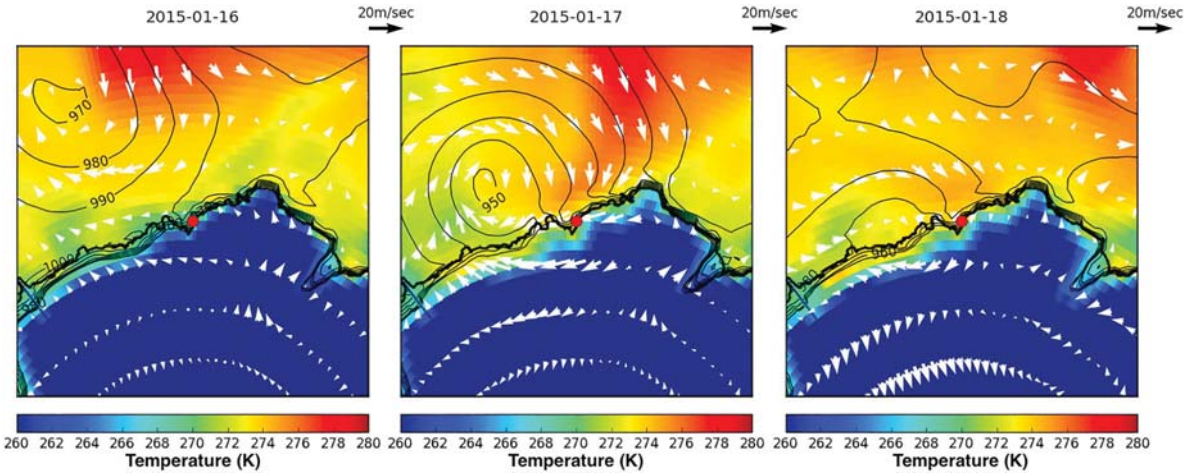

Figure 3. Surface air temperature (colors), surface pressure (contours), and wind (vectors) of the European Centre for Medium-Range Weather Forecasts Interim Re-Analysis data set at 0000 UTC for (a–c) 16–18 January 2015 for the immediate surroundings of Syowa Station (red circle).

Courant-Friedrichs-Lewy criterion and varies with latitude and horizontal wind velocity. We analyzed trajectory by employing a kinematic trajectory method and calculated the course of movement of the air mass that drifted above Syowa Station at an altitude of 100 m for 2 days, beginning at 0000 UTC on 17 January.

3. Results

In this section, we describe the strong wind event that occurred on 17 January 2015 using the WRF. The WRF results are first compared with observations to ensure accuracy. Then, three-dimensional atmospheric fields surrounding the strong wind portion are investigated to clarify the dynamical structure. To evaluate the horizontal and vertical wind conditions, we use the coarse domain. For point evaluations, such as comparisons with observations, the fine domain is generally used. To target the effect of the slope in detail, the fine domain is used for longitude-height cross-section analysis.

3.1. Validation of Model Results

The simulation results are first compared with radiosonde observations at Syowa Station, which are normally taken at 0000 and 1200 UTC. Unfortunately, 0000 UTC on 17 January, at the mature stage of the wind event, the radiosonde was not launched because the wind was too strong. Figure 4 shows a comparison of the vertical profiles of air temperature, horizontal wind speed, and wind direction between radiosonde observations and the mean of the nearest nine grid points of the WRF simulation using the fine domain at 1200 UTC on 17

Table 1
Settings for WRF Calculations

Term	Coarse (Domain-01)	Fine (Domain-03)
Time step	180 s	
Vertical level	61 eta levels	
Spatial resolution	30 km	3.3 km
Radiative transfer	RRTMG for longwave and Goddard for shortwave	
Boundary layer	Mellor-Yamada-Janjić	
Surface layer	Monin-Obkhov scheme	
Microphysics	WSM5 scheme	
Cumulus parameterization	Kain-Fritsch parameterization	No parameterization
Vertical velocity damping	Not applied	
Nudging	Not applied	

Note. RRTMG = Rapid Radiative Transfer Model—Global; WRF = Weather Research and Forecasting model; WSM5 = WRF Single Moment 5 Class.

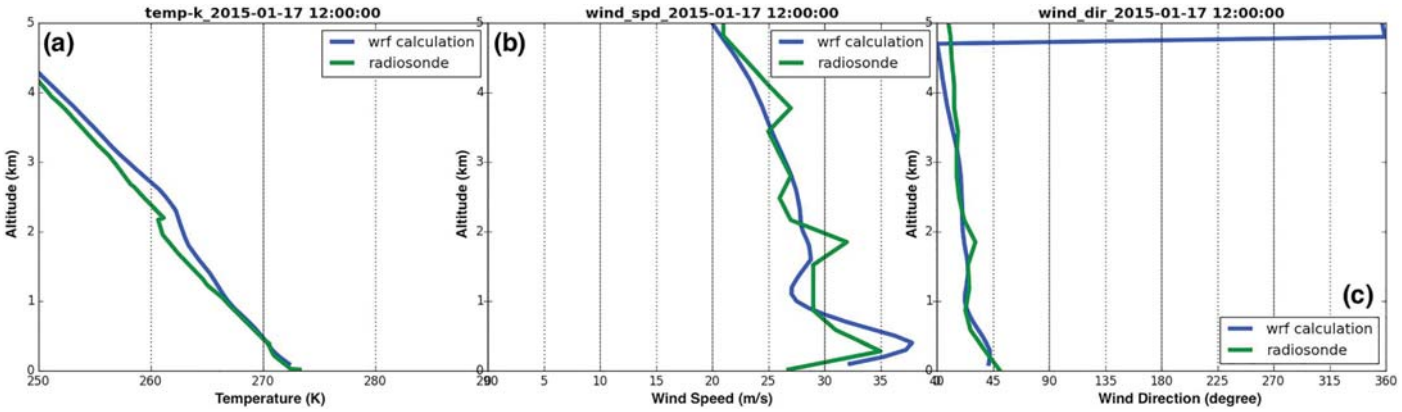

Figure 4. Comparison between Weather Research and Forecasting model simulation in the fine domain (blue) and radiosonde observations (green) of vertical distributions of (a) air temperature, (b) horizontal wind speed, and (c) wind direction.

January. The WRF successfully reproduced the vertical profiles of air temperature, wind speed, and wind direction. In air temperature (Figure 4a), the radiosonde detected a thin temperature inversion layer around 2 km above the surface, while in the WRF profile there was a layer with smaller lapse rate around the same altitude, although not an inversion. In wind speed (Figure 4b), WRF successfully reproduced a layer of strong wind in the boundary layer, with a speed of 37.8 m/s at 400 m (930 hPa), which was observed as 35 m/s and 281 m (943 hPa) by the radiosonde. Fluctuations in wind speed above 1-km altitude were not reproduced exactly by WRF, but the tendency with height was largely consistent with the observations. The surface wind direction is northeast at the surface in both observations and calculations (Figure 4c). The direction becomes north-northeast at around 1-km height, and it exhibits an anticlockwise rotation with increasing height. Thus, the WRF successfully reproduces the observed temperature and wind.

Figure 2 compares the modeled (bottom-of-atmosphere fine domain) and observed surface pressure, air temperature, horizontal wind speed, and wind direction during the strong wind event. Both the model and the observations show decreasing surface pressure from approximately 0600 UTC on 16 January as the depression approaches. The minimum pressure was observed at 0000 UTC on 17 January, while in the model results the lowest value developed from 16 January at 2000 UTC to 17 January at 0600 UTC. The pressure and temperature of the model are consistent with observations. Wind speed is also approximately consistent with observations, but the model sometimes underestimates wind speed before a strong wind event. When wind speeds are significantly underestimated, modeled wind direction also differs from observations. However, after the strong wind event at 0000 UTC on the 17th, both wind speed and direction are consistent with observations. Overall, the WRF calculation was successful in reproducing the strong wind event.

3.2. Horizontal Analysis

Figure 5 shows the surface wind at 0000 UTC from 15 to 19 January 2015 in the coarse domain. In this period, a depression accompanied by cyclonic flow was located west of Syowa Station. The pressure at the center of the depression was less than 970 hPa before 0600 UTC 16 January, and the depression approached Syowa Station with deepening central pressure and intensifying circulation. At 0000 UTC on 17 January, the central pressure of the depression was lower than 950 hPa. After the event, from 0000 UTC of 18 and 19 January, the depression weakened rapidly. On 19 January the depression disappeared.

Figure 6 illustrates wind and potential temperature on the 950, 850, 700, and 600 hPa isobaric surfaces at 0000 UTC on 17 January, when the surface wind was the strongest. At this time, warm air to the east of the depression flowed clockwise from southeastward to southward at all altitudes. There was an extended region of cold air between the warm air migrating southward and the ice sheet slope surface. The region of cold air approximately coincided with the strong easterly wind, which was located over Syowa Station and the sea-ice area at the 950-hPa level, over the tip of the ice sheet at 850 hPa, and over the lower slope of the ice sheet at 700 hPa. At 600 hPa, a moderate strong wind developed on the ice sheet beyond the migrating warm air. Therefore,

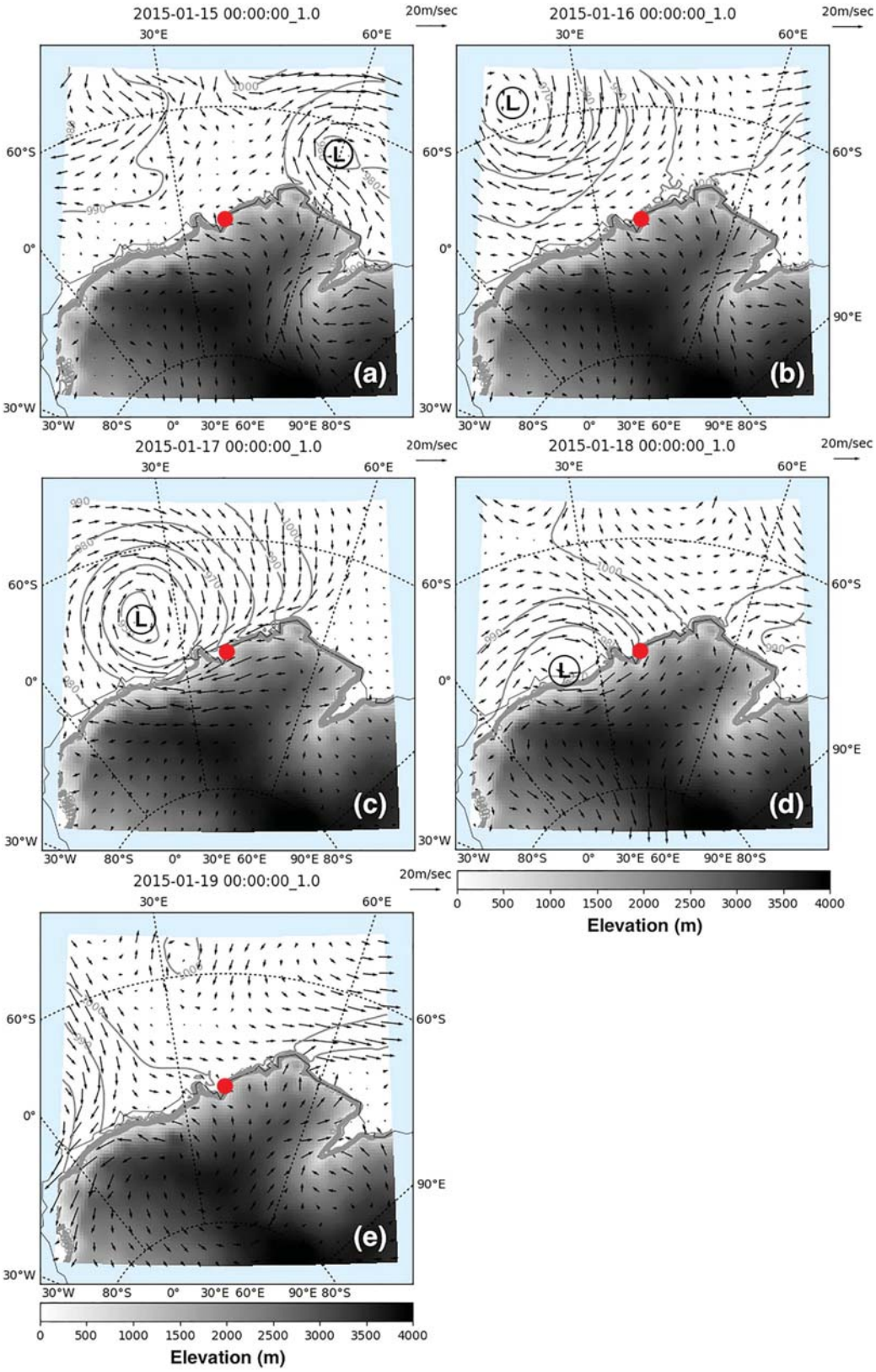

Figure 5. Surface wind (vectors), elevation (shading), and pressure (contours) in the rough domain at 0000 UTC on 15 (a), 16 (b), 17 (c), 18 (d), and 19 (e) January 2015.

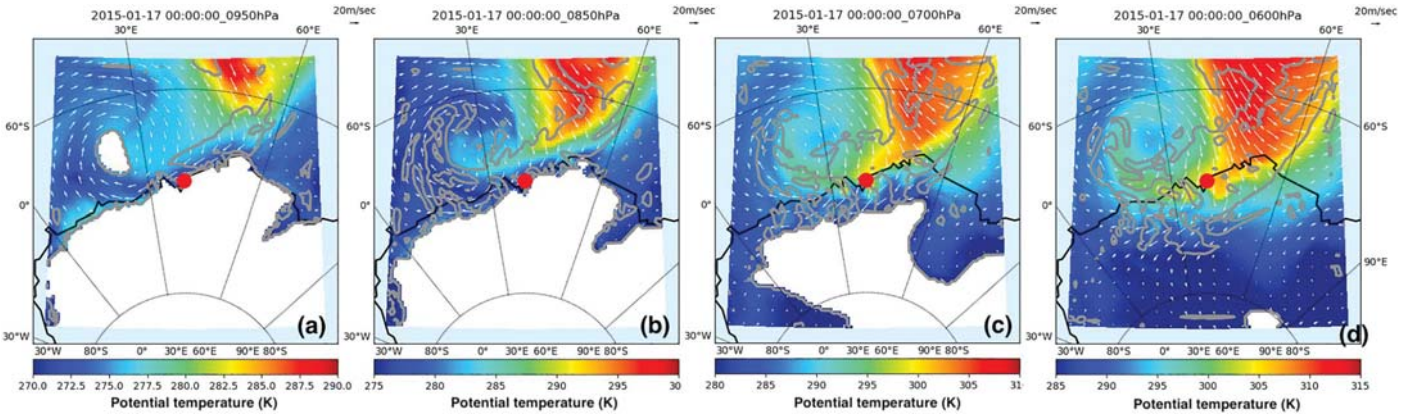

Figure 6. Horizontal wind (vectors), potential air temperature (orange shading), and vertical wind (contours) in the coarse domain at 0000 UTC on 17 January 2015 on the 950 (a), 850 (b), 700 (c), and 600 hPa (d) isobaric surfaces. Contours show only the region of large vertical upward wind (>0.01 m/s), which is surrounded by bold lines. Note that the color bars are different at different pressure levels. Red circle indicates Syowa station. White regions mean no data at the isobaric levels.

Syowa Station was located under the extended region of cold air at the lower altitudes of 950 and 850 hPa, and covered by the warm air migrating southward at the higher altitudes of 700 and 600 hPa. The southern end of the warm migration corresponds to the region of strong upwelling.

The characteristics of the easterly wind and the cold air region along the ice sheet surface and meridional localized spacing are more prominent in the lower layers at 950 and 850 hPa than in the upper levels. Note that ascending motion prevails in the southern part of the region where warm air migrates into the region of cold air. The situation corresponds to the *orographic blocking* discussed by Schwerdtfeger (1975) in the context of the formation of an southerly jet in the lower troposphere on the eastern side of the Antarctic Peninsula.

In the present case at Syowa Station, the steep topography of the ice sheet plays the role of the peninsula in Schwerdtfeger's case. Namely, the ice sheet slope blocks the northerly flow accompanying the cyclone and deflects the flow along the ice sheet surface. To describe the relationship between atmospheric boundary conditions and the terrain barrier, two scaling parameters are calculated: the Rossby deformation radius (R) and the Froude number. The former is an e-folding scale that determines the horizontal distance across which the presence of mountains influences cyclone dynamics. R is defined as follows:

$$R = \left(gH\frac{\Delta\theta_b}{\theta_b}\right)^{1/2}\left|\frac{1}{f}\right|, \tag{1}$$

where f is the Coriolis parameter (-1.43×10^{-4} s^{-1}), H is the depth of the boundary layer, θ_b is the average potential temperature of the layer, and $\Delta\theta_b$ is the potential temperature increase between the boundary layer and the layer above. For summer boundary-layer conditions at Syowa Station, H is typically 1.2 km on average (Hayashi et al., 2012). Under strong-wind conditions, $\Delta\theta_b$ and θ_b are 7.9 and 307.9 K, respectively. Thus, R under strong-wind conditions is 121 km. Thus, as can be seen from Figure 1, it is clear that barrier flow exists within a band along the northwest of the ice shelf of this approximate width.

The Froude number, Fr, is used to describe how an atmospheric flow interacts with an obstacle and is the ratio of the kinetic energy of a parcel to the potential energy to be overcome by crossing a barrier of a specific height. Fr is defined as follows:

$$Fr = U_0\left(gh\frac{\Delta\theta}{\theta}\right)^{-1/2}, \tag{2}$$

where U_0 is the wind speed in the direction approaching the obstacle, g = 9.8 m/s^2, h is the altitude of the terrain obstacle, θ is the mean potential temperature of the layer, and $\Delta\theta$ is the difference in potential

temperature from the surface to h. When $0 < Fr < 1$, air at the surface lacks the kinetic energy to flow over the obstacle and the flow is deflected. The height of the ice sheet (h) is determined for the point at R = 1,500 m from Syowa station. During the strong wind event of 0000 UTC p.m. 17 January, θ = 279.3 K and $\Delta\theta$ = 7.5 K on the slope at 880 m over the ice sheet. The marine wind speed, which is caused by the depression and the nearly northern flow in the region from 39°E to 41°E and 60°S to 66°S, north of Syowa, is 13.4 m/s. Equation (2) results in an Fr of 0.67 for the surface flow and during the strong wind event the flow is deflected by the steep topography.

On the slope south of Syowa Station, the altitudes of 850, 700, and 600 hPa are approximately 1,100, 2,640, and 3,850 m, respectively. Thus, the flows at 600 and 700 hPa pass above the surface at 1,500 m. Over the northern sea of Syowa where wind directions are approximately northerly, wind speed is 24.7 m/s at 850 hPa. The potential temperature is 267.4 K, and the difference in potential temperature is 7.4 K at 850 hPa. The Fr over the slope at 850 hPa is 0.66 and the northerly wind does not have enough kinetic energy to cross the steep topography. Thus, layers up to around a height of 1.5 km are readily influenced by topography. However, upper layers, which are affected by warm migration caused by depressions (as shown in Figure 6), are unaffected by topography.

3.3. Latitude-Height Cross-Section Analysis

The upwelling in the southern part of the migrating warm air is important for formation of the narrow cold region along the ice sheet as air with lower potential temperature originated from the east of Syowa station from the lower layer, which is unaffected by warm migration, is lifted up. The perturbation in the temperature field caused by the upwelling can immediately be seen in the mesoscale horizontal pressure field. Migration of warm air above the sea and relatively cold air along the slope lead to a pressure gradient that is approximately perpendicular to the contours of ice sheet elevation, which consequently accelerates the easterly wind at the lower levels to reach a balance consistent with the thermal wind relationship. In the section, such dynamical relations between temperature, and pressure and wind fields will be discussed with reference to fine spatial structures in the latitude-height cross section. Figure 7 shows latitude-height cross sections of potential temperature, wind, and pressure at 0000 UTC from 16 to 18 January in the coarse domain. The cross sections cut the coastline to the east of Syowa Station to avoid the complex effects of the bay-shaped coastline around the station (Figure 1). As the exact wind direction is approximately along the coastline or along the contours of the elevation of the ice sheet, the wind is separated into two components, one with direction parallel (U') and one orthogonal (V') to the coastline. In fact, U' is tilted 30° to the north from the conventional east-west U component, and V' is tilted 30° to the west from the usual V component.

When the wind speed at Syowa is the strongest on 0000 UTC 17 January, a prominent negative U′, equivalent to the strong easterly wind (dashed contours in Figure 7b) prevails above the lower part of the ice sheet slope from the surface to approximately 3-km altitude. The strongest wind is elevated from the surface. Considering the spatial features of the strong wind together with its narrow latitudinal extent, it can be referred to as a low-level jet. Comparison with Figures 7a and 7c shows that the downslope wind, corresponding to the katabatic wind, was also enhanced under the low-level jet.

The prominent negative U′ is located in the temperature inversion layer on the surface of the ice sheet slope. The inversion is formed by a combination of warm air advection at higher altitudes (700 and 600 hPa) and the narrow cold zone at lower altitudes (950 and 850 hPa), as shown in Figure 6. The amplitude of the temperature inversion is approximately 6 K between 2.5 km and the surface.

Note that the potential air temperature at and around the prominent negative U′ is higher on 0000 UTC 17 January than before (Figure 8a) or after (Figure 8c). Namely, this strong wind event occurred under robust warm air advection in the upper atmosphere and resulted in a temperature inversion field. In this situation, the colder air of the inversion, which came from the east, is formed mainly by air with lower potential temperature from the lower layer, which is supplied by the upwelling that develops around the southern end of the migrating warm air. Considering the relative location of the upwelling and the ice sheet slope, the motion occurs as a result of the barrier effect of the ice sheet slope, which is the most important process for orographic blocking.

The pressure field is also illustrated in Figure 7. On 17 January, the pressure gradient reverses around 67°S. North of 67°S the pressure gradient is positive; that is, higher pressure to the north (red color in Figure 8f).

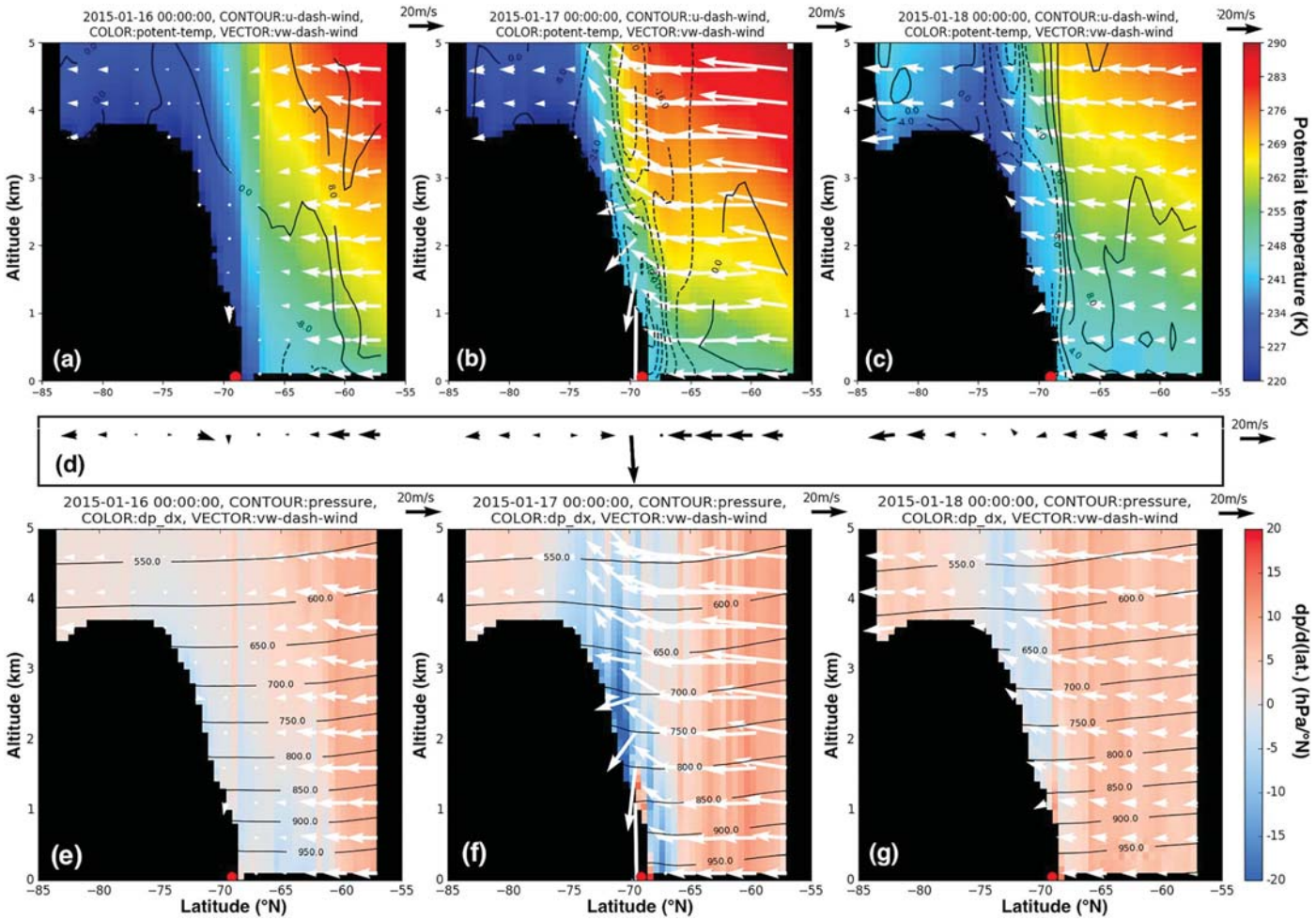

Figure 7. Latitude-height cross sections for 40.6–42.6°E in the coarse domain at 0000 UTC on 16 (left), 17 (middle), and 18 (right) January 2015. Arrows indicate wind vectors (V', 100*W), in the form V' + 100-W wind. U′ (contours) and potential temperature (color) are shown in upper panels. Lower panels show pressure (contours) and pressure gradient, $\partial p/\partial$[lat] (color). Black arrows in the center panel indicate surface wind. The red circle indicates the latitudinal position of Syowa station, which lies outside of the longitudinal range of the cross section.

While the positive pressure gradient in the northern half of the cross section changes little over the 3 days, the negative pressure gradient south of 67°S is notable in the near-surface layer over the ice sheet slope only on 17 January. The negative pressure gradient apparently contributes to the strong easterly wind. The combination of the negative pressure gradient and the negative U′ corresponding to the easterly wind is the geostrophic wind relationship in the Southern Hemisphere.

Geostrophic wind, V_g, at a point with latitude φ between two points with distance Δn is calculated as follows:

$$V_g = -\frac{1}{2\rho\Omega \sin\phi}\frac{\Delta p}{\Delta n}, \tag{3}$$

where Ω is the angular velocity at the equator ($7.29 \times 10^{-5}\ s^{-1}$), ρ is the air density, and Δp is the pressure gradient. At 0000 UTC on 17 January, the Δn distance between two points to the south-southeast (69.1°S, 39.7°E) and north-northwest (68.5°S, 39.0°E) is ~72 km. The Δp is ~4.4 hPa near the surface. Thus, V_g at the surface is ~36.6 m/s, which is close to the wind speed observed at Syowa Station. At altitudes of 1,100, 2,460, and 3,850 m (corresponding to 850, 700, and 600 hPa, respectively) above Syowa Station, Δp values are approximately 1.7, −0.8, and −1.5 hPa, respectively. Thus, V_g at 850 hPa is 16.5 m/s. Over 700 hPa, V_g becomes negative. Easterly wind speeds decrease with increasing altitude above Syowa Station, as shown in Figure 7.

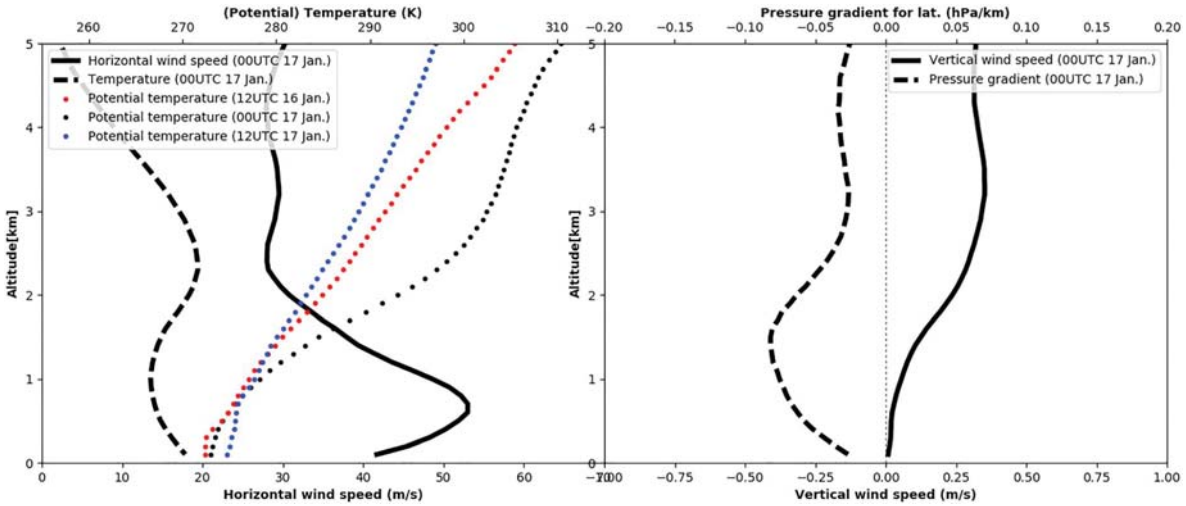

Figure 8. Vertical profile of (left panel) horizontal wind speed (solid line), air temperature (dashed line), potential air temperature (dotted line), (right panel) vertical wind speed (solid line), and pressure gradient (dashed line) along latitude from 68.4 to 68.1°S in the fine domain over Syowa station at 0000 UTC on 17 January 2015. Potential air temperature is also shown for the 12 hr before (red) and after (blue) 0000 UTC on 17 January.

Barrier wind occurs when stable flow is directed toward a topographic barrier. If the atmosphere is stably stratified and the flow does not have enough kinetic energy to cross the topography, the barrier blocks the flow and mass convergence is increased. The obstruction leads to a high-pressure field at the bottom of the topography. The high pressure decreases with separation from the barrier, and a pressure gradient is formed along the topography. Around the barrier, strong winds (corner winds) occur under the approaching cyclone because of the combination of the pressure gradient force, the Coriolis force, and the flow from the depression. The strong wind is asymmetric and accelerated on the right side of the topography in the Southern Hemisphere as a jet. This asymmetric jet was referred to as the *barrier wind corner jet* by Nigro et al. (2012), who investigated Ross Ice Shelf air stream caused by a barrier parallel flow along the base of the Transantarctic Mountains. The pressure gradient field of the present study is thought to be constructed by the barrier wind corner jet, similar to the process described by Nigro et al. (2012).

Figure 8 shows vertical profiles of atmospheric conditions for the area with the prominent negative U′ around Syowa Station during the strong wind event in the fine domain. In the layer from approximately 1- to 3-km altitude, the easterly wind speed increases with decreasing altitude, accompanied by strengthening of the negative pressure gradient as cold air piles up below 2.5-km altitude. This is consistent with the thermal wind relationship. Furthermore, the upwelling at all levels in the right panel of Figure 8 suggests uplifting of air with lower potential temperature from lower altitudes. Figure 8 also shows the potential temperature 12 hr before and after the strong wind event. During the event, although the vertical gradient of potential temperature is much greater than both before and after the event at altitudes between 1.0 and 2.5 km, the potential temperature of the boundary layer is not noticeably different before and after the event, as a result of an upwelling flow north of Syowa Station and intruding colder air from the east, which climbs up the southern topography. Negligible vertical winds exist at the bottom of the atmosphere but winds around Syowa Station are noticeable and are generally directed upward. The strongest upwelling occurs around 3-km altitude at the top of the temperature inversion. This is also found in Figure 8b. The upwelling there essentially strengthened the temperature gradient three-dimensionally.

The geostrophic wind, and thus the thermal wind, is representative in the free-atmosphere than in the boundary layer, where surface friction occurs. In this context, it is reasonable that the highest wind (the low-level jet) speed of 53.6 m/s appears at an altitude of 0.7 km, located in the transition layer between the free troposphere and the boundary layer. The strong wind of around 40 m/s at the surface appears as a lower part of the low-level jet.

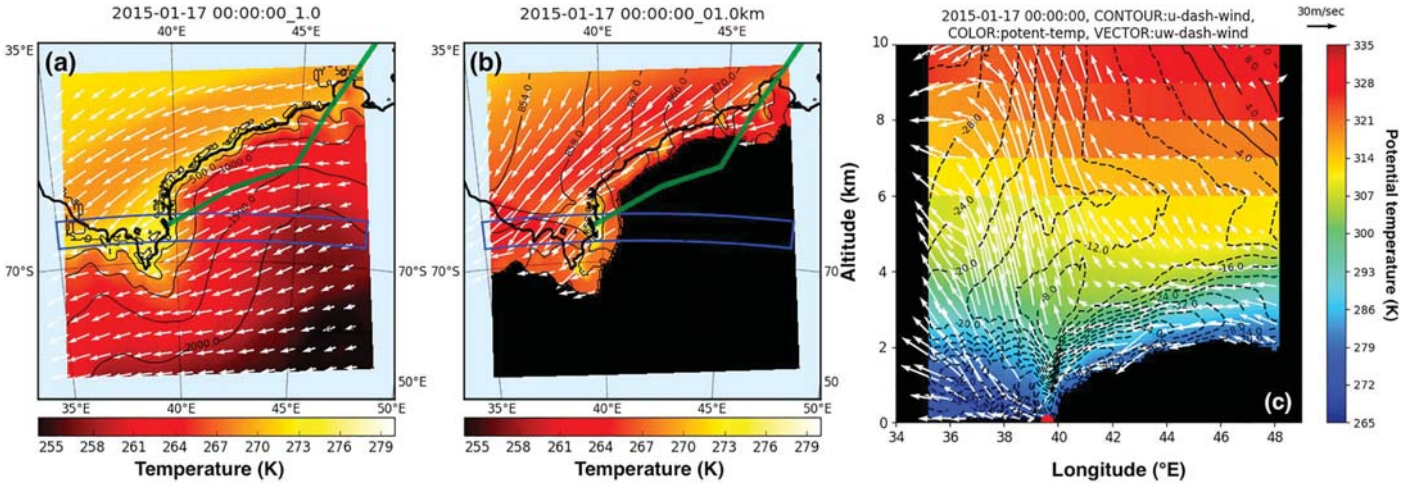

Figure 9. (a) Surface air temperature (red shading), surface elevation of the ice sheet (contours), and surface horizontal wind (white vectors) in the fine domain. Green lines indicate the track of the back trajectory analysis at an altitude of 100 m. (b) Air temperature at an altitude of 1 km in the fine domain. The region with ice sheet higher than 1 km is indicated by black shading. Green lines are the same as in (a). (c) Longitude-height cross section of wind vectors (U′ + 100-W wind), potential temperature (colors), and U′ (contours) from 0 to 10 km at 0000 UTC on 17 January 2015 in the fine domain. Vertical resolution above 5 km is 10 times coarser than that below. The red circle indicates the longitudinal position of Syowa station, which lies outside of the meridional range of the cross section.

3.4. Longitude-Height Cross-Section Analysis and Vertical Wind Event

Figure 9a shows the distribution of surface air temperature around Lutzow-Holm Bay during the strong wind event on 17 January in the fine domain. The inner part of the bay was warmer than the area north of the bay. On the horizontal surface at 1-km altitude (Figure 9b), a locally warmer area appeared at the foot of the ice sheet to the south of Syowa Station. According to a back trajectory analysis, the warm air-mass descended from the eastern slope of the ice sheet. As this phenomenon has already been pointed out or analyzed in association with strong wind events, the mechanism responsible will be clarified here.

Figure 9c shows longitude-height cross sections of potential air temperature, U′ + 100-W wind, and U′ at 69.3–69.7°S (see Figure 1) on 17 January 2015 at 0000 UTC. In the lower troposphere, there was strong easterly flow down the ice sheet surface. Air temperature in the flow increased on the downstream side, apparently due to adiabatic heating of descending air with higher potential temperature from higher altitudes. The locally warmer area found at the ice surface at 1-km altitude was formed by penetration of descending air into the flow trapped in the boundary layer on the ice sheet surface. Then, the flow touched down on the surface of the bay and warmed the whole area while spreading out. Namely, a kind of foehn occurred there during the strong wind event. The downstream portion of the air mass with high potential temperatures effected an end to the cold temperatures along to the slope, leading to a strong wind event. As seen in the latitude-height cross section of the strong wind event in Figure 8f, there is a region with an inverse trend in the pressure gradient (i.e., pressure is higher in the north; reddish color in the figure) at 1.0 to 1.5 km along the slope compared with vertically adjacent altitudes. The northern higher-pressure region caused by a downflow of warm potential temperatures may have weakened the wind speeds over Lutzow-Holm Bay. Because of the location of the bay, Syowa Station is affected by both foehn and synoptic influences. In the strong wind event considered here, the easterly wind blowing over the ice sheet was dragged down along the surface from an altitude of around 3 km to near the surface at the foot of the ice sheet. This region is also frequently affected by downslope flow giving katabatic wind. Note that since katabatic wind occurs only in the boundary layer on the ice sheet surface, the record wind event described here is essentially a different phenomenon from a simple katabatic wind regime.

4. Summary and Remarks

This study investigated the strong wind event observed at Syowa Station on 17 January 2015, which broke the January wind speed record with maximum mean wind speed of 41.8 m/s and gusts up to 51.4 m/s.

Historically, 95% of wind speeds at Syowa Station are lower than 21 m/s and the present case is the only one with a maximum wind reaching 40 m/s.

A numerical model, the WRF, reproduced successfully important features of the event: (1) strong wind at Syowa Station in association with the approach of a synoptic-scale depression and (2) a strong easterly wind was more prominent in the lower troposphere at the 950- and 850-hPa levels than in the upper layers. Thus, the atmospheric structure simulated by WRF was suitable for analysis to investigate how the strong wind was established.

The strong easterly wind developed along the contour lines of the ice sheet slope from approximately 50°E to 30°E, corresponding to the southern edge of the warm air migrating southward in the circulation associated with the synoptic-scale depression. However, the warm air did not occupy completely the path of the strong easterly, and a narrow zone of relatively cold air remained along the strong easterly wind. The strong easterly wind developed consistently with the negative meridional pressure gradient in this region, and this negative pressure gradient was consistent with a positive temperature gradient that corresponded to the combination of migrating warm air and persistent cold air. The cold air is thought to have originated in lower layers with lower potential temperature, as upwelling prevailed there. Both the temperature gradient and pressure gradient were stronger in the lower layer, and the easterly wind strengthened with decreasing altitude, satisfying the thermal wind relationship. All the characteristics of the present case are consistent with orographic blocking.

While the mechanism of orographic blocking has already been thought relevant to aspects of Antarctic circulation, such as the lower tropospheric southerly jet on the eastern side of the Antarctic Peninsula (Schwerdtfeger, 1975) and the Antarctic surface wind regime (Parish & Cassano, 2003), this study indicates that orographic blocking is effective in generating strong wind along the coastal edge of the Antarctic ice sheet. Moreover, the nonhydrostatic model employed here showed directly that northerly flow climbs up the slope of the ice sheet and then forms a region of cold air along the edge of the ice sheet. A strengthening of the katabatic wind was diagnosed in the model in the region below the air ascending the ice sheet. This study indicates that the region around Lutzow-Holm Bay also undergoes topography-influenced blocking similar to the blocking wind corner jet of Nigro et al. (2012) around the Transantarctic Mountains.

A new finding of this study is the heating of surface air in Lutzow-Holm Bay during the strong wind event. This was accompanied by descending motion from a height of approximately 3 km down the slope of the ice sheet; that is, a kind of foehn. The descending flow penetrates through a narrow zone just above the ice sheet surface and spreads out over the sea surface of Lutzow-Holm Bay. Ascending motion also developed up the slope of the ice sheet to the west of the bay, which was evident up to the tropopause. While the mechanism of warming may be understood as a foehn, that of upwelling in the extended region toward the west of the ice sheet is still unclear. A greater understanding of this upwelling may come from a comparison with the hydraulic jump during the strong wind event investigated by Tomikawa et al. (2015).

Acknowledgments
The production of this paper was supported by the National Institute of Polar Research (NIPR) publication subsidy. Surface and vertical observation data at Syowa Station were distributed as part of the past observation data set of the Japan Meteorological Agency (http://www.data.jma.go.jp/obd/stats/etrn/). ERA-Interim results were downloaded from the ERA-Interim, Daily (http://apps.ecmwf.int/datasets/data/interim-full-daily). The global analysis and forecast data of the National Centers for Environmental Prediction (NCEP) Final Analysis (GFS-FNL) were obtained from the NCAR Research Data Archive (https://rda.ucar.edu/datasets/ds083.2/).

References

Adams, A. S. (2005). The relationship between topography and the Ross Ice Shelf air stream, (PhD thesis). (125 pp.). University of Wisconsin—Madison.

Bintanja, R. (1998). The contribution of snowdrift sublimation to the surface mass balance of Antarctica. *Annals of Glaciology*, *27*, 251–259. https://doi.org/10.3189/1998AoG27-1-251-259

Bromwich, D. H., Robasky, F. M., Cullather, R. I., & van Woert, M. L. (1995). The atmospheric hydrologic cycle over the Southern Ocean and Antarctica from operational numerical analyses. *Monthly Weather Review*, *123*(12), 3518–3538. https://doi.org/10.1175/1520-0493(1995)123<3518:TAHCOT>2.0.CO;2

Chenoli, S. N., Turner, J., & Samah, A. A. (2013). A climatology of strong wind events at McMurdo station, Antarctica. *International Journal of Climatology*, *33*(12), 2667–2681.

Chenoli, S. N., Turner, J., & Samah, A. A. (2015). A strong wind event on the Ross Ice Shelf, Antarctica: A case study of scale interactions. *Monthly Weather Review*, *143*(10), 4163–4180. https://doi.org/10.1175/MWR-D-15-0002.1

Dee, D. P., Uppala, S. M., Simmons, A. J., Berrisford, P., Poli, P., Kobayashi, S., Andrae, U., et al. (2011). The ERA-interim reanalysis: Configuration and performance of the data assimilation system. *Quarterly Journal of the Royal Meteorological Society*, *137*(656), 553–597. https://doi.org/10.1002/qj.828

Hayashi, M., Umemoto, S., Hara, K., & Higashino, S. (2012). Vertical distributions of aerosol concentrations in the troposphere and the lower stratosphere over Syowa Station, Antarctica during the summer. Symposium on Aerosol Science & Technology, 9th, 57–58.

Hirasawa, N., Nakamura, H., Motoyama, H., Hayashi, M., & Yamanouchi, T. (2013). The role of synoptic-scale features and advection in prolonged warming and generation of different forms of precipitation at Dome Fuji station, Antarctica, following a prominent blocking event. *Journal of Geophysical Research: Atmospheres*, *118*, 6916–6928. https://doi.org/10.1002/jgrd.50532

Hirasawa, N., Nakamura, H., & Yamanouchi, T. (2000). Abrupt changes in meteorological conditions observed at an inland Antarctic station in association with wintertime blocking formation. *Geophysical Research Letters*, *27*(13), 1911–1914. https://doi.org/10.1029/1999GL011039

Hong, S. Y., Dudhia, J., & Chen, S. H. (2004). A revised approach to ice microphysical processes for the bulk parameterization of clouds and precipitation. *Monthly Weather Review*, *132*(1), 103–120. https://doi.org/10.1175/1520-0493(2004)132<0103:ARATIM>2.0.CO;2

Hoskins, B. J., & Hodges, K. I. (2005). A new perspective on Southern Hemisphere storm tracks. *Journal of Climate*, *18*(20), 4108–4129. https://doi.org/10.1175/JCLI3570.1

Janjić, Z. I. (1990). The step-mountain coordinate: Physical package. *Monthly Weather Review*, *118*(7), 1429–1443. https://doi.org/10.1175/1520-0493(1990)118<1429:TSMCPP>2.0.CO;2

Knuth, S. L., & Cassano, J. J. (2011). An analysis of near-surface winds, air temperature, and cyclone activity in Terra Nova Bay, Antarctica, from 1993 to 2009. *Journal of Applied Meteorology and Climatology*, *50*(3), 662–680.

Kodama, Y., Wendler, G., & Ishikawa, N. (1989). The diurnal variation of the boundary layer in summer in Adélie Land, eastern Antarctica. *Journal of Applied Meteorology*, *28*(1), 16–24. https://doi.org/10.1175/1520-0450(1989)028<0016:TDVOTB>2.0.CO;2

National Centers for Environmental Prediction/National Weather Service/NOAA/U.S. Department of Commerce (2000). NCEP FNL Operational Model Global Tropospheric Analyses, continuing from July 1999. https://doi.org/10.5065/D6M043C6. Research Data Archive at the National Center for Atmospheric Research, Computational and Information Systems The Laboratory, Boulder, Colo. (Updated daily.) Accessed 04 Apr. 2016.

Nigro, M. A., & Cassano, J. J. (2014). Identification of surface wind patterns over the Ross Ice Shelf, Antarctica, using self-organizing maps. *Monthly Weather Review*, *142*(7), 2361–2378. https://doi.org/10.1175/MWR-D-13-00382.1

Nigro, M. A., Cassano, J. J., Lazzara, M. A., & Keller, L. M. (2012). Case study of a barrier wind corner jet off the coast of the Prince Olav Mountains, Antarctica. *Monthly Weather Review*, *140*(7), 2044–2063. https://doi.org/10.1175/MWR-D-11-00261.1

O'Connor, W. P., Bromwich, D. H., & Carrasco, J. F. (1994). Cyclonically forced barrier winds along the Transantarctic Mountains near Ross Island. *Monthly Weather Review*, *122*(1), 137–150. https://doi.org/10.1175/1520-0493(1994)122<0137:CFBWAT>2.0.CO;2

Orr, A., Phillips, T., Webster, S., Elvidge, A., Weeks, M., Hosking, S., & Turner, J. (2014). Met Office unified model high-resolution simulations of a strong wind event in Antarctica. *Quarterly Journal of the Royal Meteorological Society*, *140*(684), 2287–2297.

Parish, T. R., & Bromwich, D. H. (1987). The surface windfield over the Antarctic ice sheets. *Nature*, *328*(6125), 51–54. https://doi.org/10.1038/328051a0

Parish, T. R., & Cassano, J. J. (2003). The role of katabatic winds on the Antarctic surface wind regime. *Monthly Weather Review*, *131*(2), 317–333. https://doi.org/10.1175/1520-0493(2003)131<0317:TROKWO>2.0.CO;2

Petterssen, S. (1940). *Weather analysis and forecasting*. New York: McGraw-Hill Book Company, Inc.

Powers, J. G. (2007). Numerical prediction of an Antarctic severe wind event with the Weather Research and Forecasting (WRF) model. *Monthly Weather Review*, *135*(9), 3134–3157. https://doi.org/10.1175/MWR3459.1

Powers, J. G., Manning, K. W., Bromwich, D. H., Cassano, J. J., & Cayette, A. M. (2012). A decade of Antarctic science support through AMPS. *Bulletin of the American Meteorological Society*, *93*(11), 1699–1712. https://doi.org/10.1175/BAMS-D-11-00186.1

Sato, K., & Hirasawa, N. (2007). Statistics of Antarctic surface meteorology based on hourly data in 1957–2007 at Syowa Station. *Polar Science*, *1*(1), 1–15. https://doi.org/10.1016/j.polar.2007.05.001

Schwerdtfeger, W. (1975). The effect of the Antarctic Peninsula on the temperature regime of the Weddell Sea. *Monthly Weather Review*, *103*(1), 45–51. https://doi.org/10.1175/1520-0493(1975)103<0045:TEOTAP>2.0.CO;2

Simmonds, I., & Keay, K. (2000). Mean Southern Hemisphere extratropical cyclone behavior in the 40-year NCEP–NCAR reanalysis. *Journal of Climate*, *13*(5), 873–885. https://doi.org/10.1175/1520-0442(2000)013<0873:MSHECB>2.0.CO;2

Simmonds, I., Keay, K., & Lim, E. P. (2003). Synoptic activity in the seas around Antarctica. *Monthly Weather Review*, *131*(2), 272–288. https://doi.org/10.1175/1520-0493(2003)131<0272:SAITSA>2.0.CO;2

Simmonds, I., & Murray, R. J. (1999). Southern extratropical cyclone behavior in ECMWF analyses during the FROST special observing periods. *Weather and Forecasting*, *14*(6), 878–891.

Simmonds, I., Murray, R. J., & Leighton, R. M. (1994). A refinement of cyclone tracking. compare.

Skamarock, W. C. (2008). A description of the advanced research WRF version 3. Tech. Note, 1–96.

Steinhoff, D. F., Bromwich, D. H., Lambertson, M., Knuth, S. L., & Lazzara, M. A. (2008). A dynamical investigation of the May 2004 McMurdo Antarctica severe wind event using AMPS*. *Monthly Weather Review*, *136*(1), 7–26. https://doi.org/10.1175/2007MWR1999.1

Tomikawa, Y., Nomoto, M., Miura, H., Tsutsumi, M., Nishimura, K., Nakamura, T., Yamagishi, H., et al. (2015). Vertical wind disturbances during a strong wind event observed by the PANSY Radar at Syowa Station, Antarctica. *Monthly Weather Review*, *143*(5), 1804–1821. https://doi.org/10.1175/MWR-D-14-00289.1

Trenberth, K. E. (1991). Storm tracks in the Southern Hemisphere. *Journal of the Atmospheric Sciences*, *48*(19), 2159–2178. https://doi.org/10.1175/1520-0469(1991)048<2159:STITSH>2.0.CO;2

Turner, J., Chenoli, S. N., Marshall, G., Phillips, T., & Orr, A. (2009). Strong wind events in the Antarctic. *Journal of Geophysical Research*, *114*, D18103. https://doi.org/10.1029/2008JD011642

Turner, J., Lachlan-Copea, T. A., Marshall, G. J., Pendlebury, S., & Adams, N. (2001). An extreme wind event at Casey Station, Antarctica. *Journal of Geophysical Research*, *106*(D7), 7291–7311. https://doi.org/10.1029/2000JD900544

Uotila, P., Vihma, T., Pezza, A. B., Simmonds, I., Keay, K., & Lynch, A. H. (2011). Relationships between Antarctic cyclones and surface conditions as derived from high-resolution numerical weather prediction data. *Journal of Geophysical Research*, *116*, D07109. https://doi.org/10.1029/2010JD015358

van As, D., van den Broeke, M. R., & Helsen, M. M. (2007). Strong-wind events and their impact on the near-surface climate at Kohnen Station on the Antarctic Plateau. *Antarctic Science*, *19*(4), 507–519.

van den Broeke, M., Reijmer, C., van As, D., van de Wal, R., & Oerlemans, J. (2005). Seasonal cycles of Antarctic surface energy balance from automatic weather stations. *Annals of Glaciology*, *41*, 131–139. https://doi.org/10.3189/172756405781813168